# Planar integrated plasmonic mid-IR spectrometer

Christopher J. Fredricksen[*a], Justin W. Cleary[b], Walter R. Buchwald[c], Pedro Figueiredo[d], Farnood Khalilzadeh-Rezaie[d], Gautam Medhi[d], Imen Rezadad[d], Monas Shahzad[d], Mehmet Yesiltas[d], Janardan Nath[d], Javaneh Boroumand[d], and Robert E. Peale[d]

[a]LRC Engineering, Inc., 9345 Chandon Dr., Orlando, FL 32825;
[b]Sensors Directorate, AFRL, Wright Patterson AFB, Dayton, OH 45433;
[c]Solid State Scientific Corporation, 27-2 Wright Rd., Hollis, New Hampshire 03049;
[d]University of Central Florida, 4000 Central Florida Blvd., Orlando, FL 32816

## ABSTRACT

The convergence of silicon photonics and infrared plasmonics allows compact, chip-scale spectral sensors. We report on the development of a compact mid-IR spectrometer based on a broad-band IR source, dielectric waveguides, a transformer to convert between waveguide modes and surface plasmon polaritons (SPP), an interaction region where analyte molecules are interrogated by SPPs, an array of ring resonators to disperse the light into spectral components, and photodetectors. The mid-IR light source emits into a dielectric waveguide, leading to a region that allows coupling of the incident photons into SPPs. The SPPs propagate along a functionalized metal surface within an interaction region, where molecular analytes cause loss at wavelengths corresponding to their characteristic vibrational modes. After a suitable propagation length, the SPP will be coupled back into a dielectric waveguide, where specific wavelength components will be out-coupled to detectors by an array of ring resonators. We have selected a 3.4 micron LED as the IR source, based on both cost and performance. Initial coupling experiments with circular waveguides formed from GLSO glass include measurement of the loss per mm. Electrodynamic simulations have been performed to inform the photonic/plasmonic transformer design. The SPP propagation length necessary for a discernible change in the signal due to absorption in the interaction region has been estimated to be on the order of 1 mm, well within the bounds of calculated propagation lengths for infrared SPPs on Au.

**Keywords:** surface plasmon, mid-IR, SOI, waveguides

## 1. INTRODUCTION

Surface plasmon polaritons (SPP) provide a promising pathway to the integration of optics and electronics, leading to ultra-high density circuitry as well as label-free measurement of analyte binding. The silicon-on-insulator (SOI) system has been proposed as an ideal platform for the integration of optics and electronics. Though unsuitable at visible wavelengths, silicon has low loss in the IR molecular fingerprint region. $SiO_2$ also has low loss between 3 and 4 microns wavelength, so that Si waveguides on $SiO_2$ should be ideal at these wavelengths. Important characteristic molecular vibrations occur in this wavelength range, namely the bond stretching modes C-H (Alkynes), O-H (monomeric alcohols, phenols) and N-H (Amines), as well as CO double bonds, $NH_2$, and CN.

The objective is a lightweight, portable spectrometer with no moving parts for molecular sensing. Currently available high resolution spectrometers are bulky, heavy, power-hungry instruments that require laboratory conditions for operation. We are working towards a robust, ultra-miniature spectrometer with resolving power that is sufficient to distinguish characteristic vibrational lines of molecular analytes. We have chosen to work at 3.4 microns wavelength, as it corresponds to many vibrational transitions in biologically and chemically important molecules.

*chris@lrcengineering.com; phone:1-386-631-7319

The device will feature an interaction region, where the analyte reacts with the SPP, which is generated just upstream by a lateral taper in the waveguide and the introduction of proximal gold surfaces (Fig. 1, left). The taper squeezes the mode out of the waveguide into the adjacent air/Au interface, achieving a photonic-to-plasmonic mode conversion. SPPs travelling along the Au/air interface may be absorbed by analytes concentrated in the channel, altering the SPP frequency content. The SPP modes are then converted back to photonic modes by another taper. Wavelengths corresponding to absorption by an analyte will be missing downstream. The mechanism for dispersing the resulting radiation will be a series of micro-ring resonators. Designed for wavelengths longer than 3 microns, the device will be ideal for chemical identification based on the vibrational spectra known for most molecules.

Figure 1 (left) presents a schematic of the prototype test bed with a single resolution channel. We are in the course of demonstrating the enabling components. Initially, light from the 3.4 micron LED will be coupled into the SOI waveguide structure using an AR coated ZnSe microscope objective. The radiation is injected into the silicon waveguide from the left and traverses the interaction region, where the photonic modes are converted to SPP, then back to photonic modes. We can confirm the action of SPPs by comparing throughput to expectations based on the known SPP propagation length for the given metal (e.g. gold) at 3.4 micron wavelength[1,2]. The micro-ring resonator couples light of its resonant frequency to an adjacent waveguide, where it is detected at the output by the external detector. In order to eliminate stray light from the source being directly incident on the detector, we introduce a 90 degree bend in the waveguide.

Fig. 1 (right) presents a schematic of the bent silicon waveguide on oxide on silicon substrate. This image establishes the coordinate system used in the electrodynamic simulations analyzing losses in the bend. Eventually, both source and detector may be integrated with the rest of the device, which would make the external IR lens and the bend unnecessary.

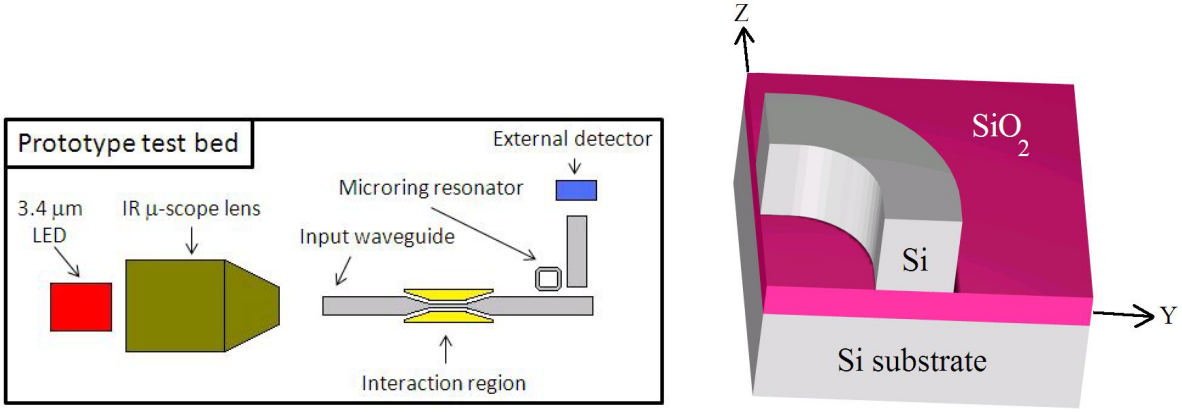


Figure 1 – (left) Schematic of the test bed device. The silicon photonic waveguide is pinched between two layers of gold, which are separated by a gap, where SPPs are expected to interact with concentrated chemical analyte. (right) Schematic of the bent silicon waveguide establishing the coordinate system used in the electrodynamic simulations.

Nearly all reports of silicon photonic waveguides and tapered SPP transformers have been performed at 1.55 microns because of the well developed technology and applications at this communications wavelength[3]. Although proposed several years ago, the first experimentally verified transmission of mid-IR radiation through SOI waveguides was just published within the past year[4]. The authors coupled 3.39 micron radiation from a HeNe laser into a bundle of single mode fibers which were butt coupled to their SOI waveguides. We focus on free space coupling of multimode radiation from a 500 μW LED with 3.4 micron center wavelength and relatively broad (~400 nm FWHM) spectral distribution. We rely on electrodynamic simulation to inform our designs.

## 2. LIGHT COUPLING

The black curve in Figure 2 (right) shows transmission through a thick GLSO fiber of 8.5 cm length, using the experimental setup shown in Figure 2 (left). The LED and microscope objective were mounted together on a translational stage and scanned in the direction shown in the figure. The fiber was then removed and the scan repeated, resulting in the red curve. The sharpness of the black curve reveals the coupling and demonstrates our set up providing IR I/O for the device under test. Our initial plan was to fabricate a mode transformer based on a tapered GLSO fiber.

To investigate this possibility, we first determined the loss of this material near 3 micron wavelengths. Transmission spectra of two GLSO slabs of different thicknesses were measured using a Fourier spectrometer. The transmission spectrum $T$ includes contributions from specular reflection $R$, scattering $S$ by surface roughness, and absorbance $\alpha d$ according to $T = (1 - R - S)\,\mathrm{Exp}[-\alpha d]$. We determine the absorption coefficient according to $\alpha = \ln(T_2/T_1)/(d_1-d_2)$. The loss in dB/mm is $10\log_{10}[\mathrm{Exp}[-\alpha\ 0.1\ \mathrm{cm}]]$, and was found to increase slightly from -1.25 dB/mm at 2500 $cm^{-1}$ to -1.35 dB/mm at 3500 $cm^{-1}$. From this it is clear that the half-power loss point (-3 dB) is nearly 3 mm, which is sufficient for our demonstration purpose. However, recent development of in-house processing capability for SOI wafers has turned our attention away from IR glasses.

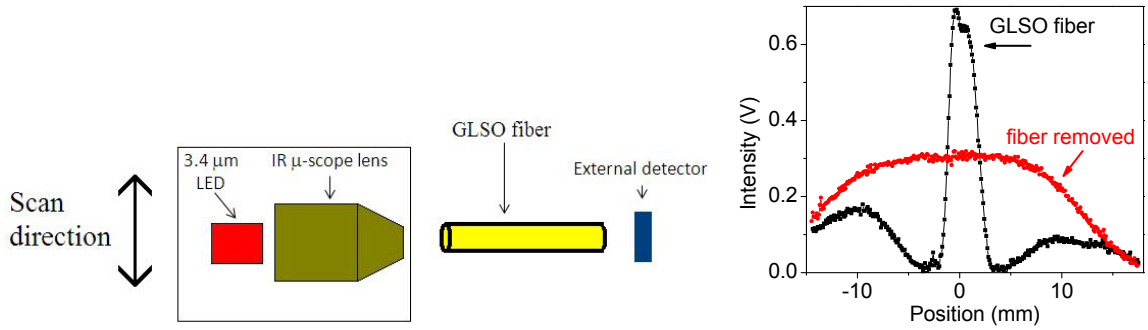


Figure 2 – (left) Experimental setup: the LED and microscope objective were mounted together on a linear translation stage and scanned laterally. (right) Curves obtained with and without a 8.5 cm long GLSO fiber in between the source and detector.

## 3. WAVEGUIDES

We initially considered a rib/slab waveguide design, with dimensions that would make it effectively single mode within a specified propagation distance[5]. Electrodynamic simulations show that our original inverted "T" shaped rib/slab waveguide design was flawed: a photon-to-plasmon transformer in the form of a lateral taper merely forces a photon mode of the desired polarization down into the slab rather than forcing it into a plasmon in the gap between the restricted rib and the metal. The solution is to etch away the arms of the "T", removing the slab and leaving a simple silicon ridge on insulator. The resulting modal structure is better confined to the desired region and it stays where it should in the transformer.

In order to eliminate the possibility of detecting light from the LED directly incident on the detector, we needed to design a waveguide with a 90 degree bend. Lumerical MODE Eigensolver software was used to model the propagation of light through waveguide bends as a function of a varying radius of curvature (ROC). The structure has a 10 micron wide x 10 micron tall Si waveguide on $SiO_2$ slab. Initial propagation is in the positive z-direction (Fig. 1, right). After passing the 90 degree bend the propagation is in the negative y-direction. The ROC is the distance from the center of curvature to the center of the waveguide (i.e. the inner and outer walls of the waveguide bends are at radii = ROC +/-5 microns).

Lumerical uses the geometry of the provided 2-D cross section to determine 100 possible propagating modes. Possible modes were first calculated for a straight waveguide. The 00 (fundamental), 11, and 22 modes are presented here as examples. The polarization lies in the plane of the bend and is perpendicular to the propagation direction. Figure 3 presents the modes as they would appear in a straight waveguide.

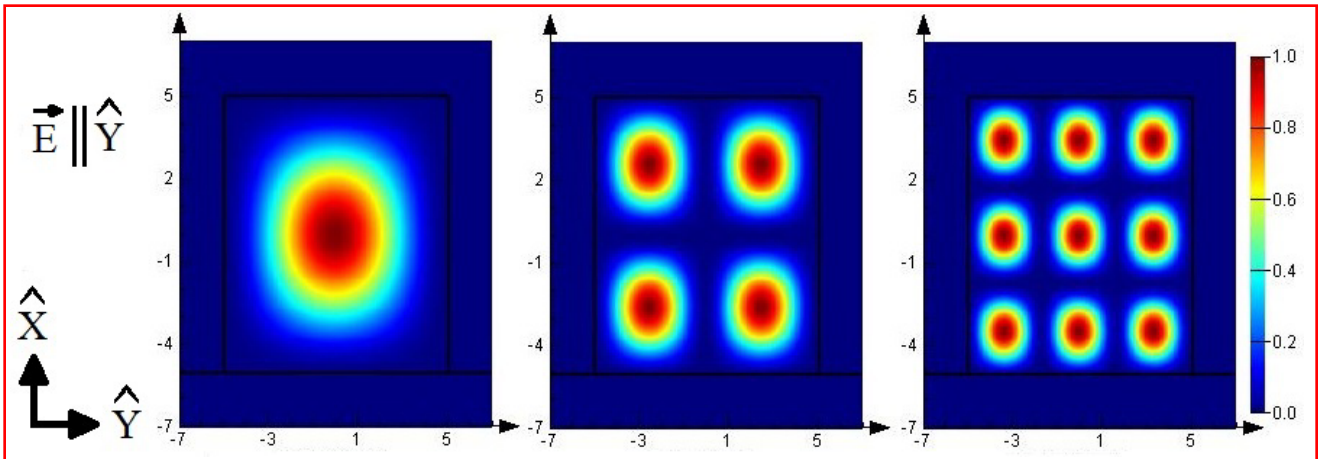


Figure 3 – From left to right, normalized field intensity of the (0, 0) (fundamental), (1, 1), and (2, 2) modes in a straight waveguide with polarization in the $E_y$ direction. The outline of the waveguide and the oxide substrate appear as black lines.

The ROC was decreased until the software could no longer register the investigated modes. This computational limit on ROC was smaller for higher order modes. Figure 4 presents three intensity plots of possible propagating modes, corresponding to modes in Fig. 3, for the limiting ROC value found for the fundamental mode. In this figure, the plane corresponds to the output of the bend (Fig 1. right) with mode now propagating in the negative y-direction. The polarization is in the z-direction after the bend. In each case, the mode becomes compressed towards the outer radius of the bend. In other words the light radiates from the bend when it becomes small, as expected.

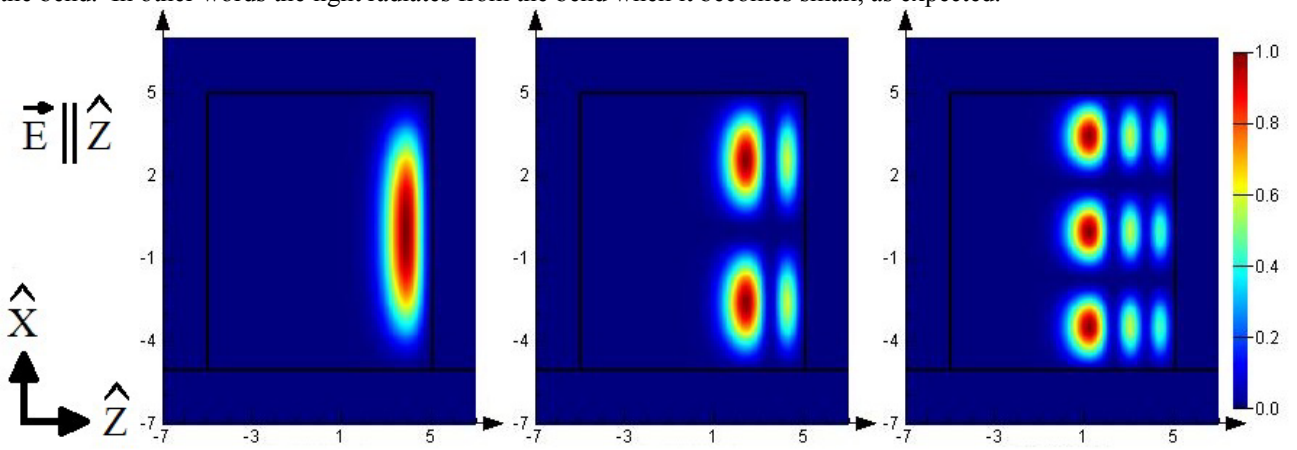


Figure 4 – From left to right, normalized intensity of the 00 (fundamental), 11, and 22 propagating modes determined for a bend with radius of 40 microns. The axes and polarization correspond to the output of the bend.

Figure 5 (left) displays a schematic of the bend with fundamental input and output mode distributions. Figure 5 (right) presents a plot of the losses determined for the investigated modes in the 90 degree waveguide bend. For a ROC of 1 mm, the losses are nearly identical to those found for the straight waveguide for each mode. Each curve in the plot ends at a small radius where the Lumerical MODE solver is no longer able to find a particular mode.

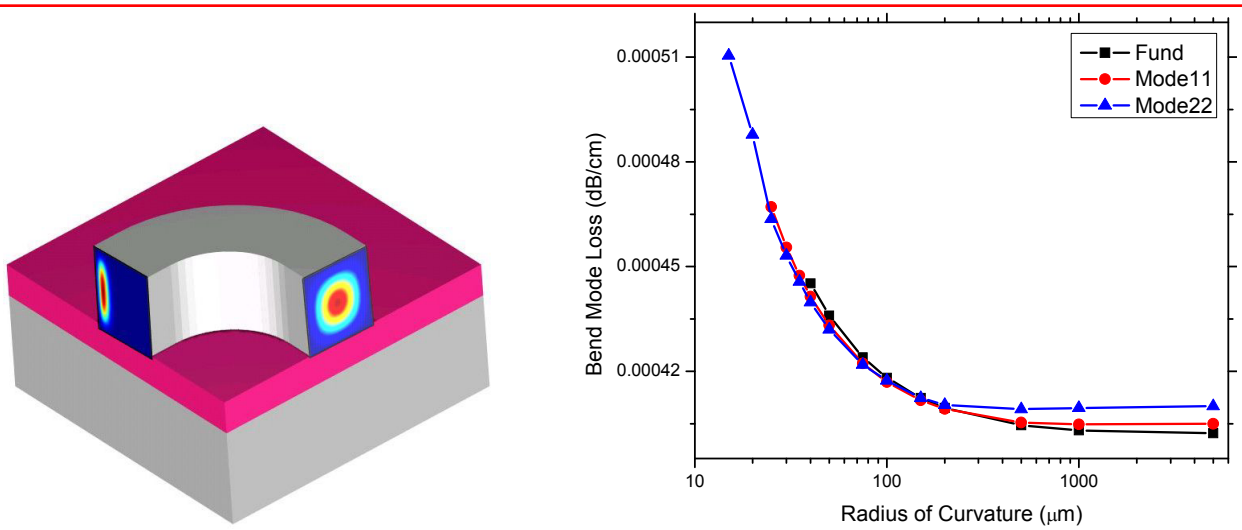


Figure 5 (left) – Schematic of silicon waveguide bend showing fundamental mode injected into the waveguide on the right and exiting on the left side, where it is compressed against the outer edge of the waveguide. (right) – Loss as a function of radius of curvature for the investigated modes.

Figure 6 presents two waveguide patterns deployed on a photolithographic mask. Figure 6 (left) contains 10 micron x 10 micron cross section waveguides with bend radii varying from 100 microns to ~2 mm. There are also several straight waveguides, including 2 that are tapered from lateral dimensions of 10 microns on the input side to 4 microns on the output side. Figure 6 (right) presents a second set of waveguides. These are identical to those of Figure 6 (left), except that they contain discontinuities surrounded by alignment marks, which are for registration during e-beam writing of the interaction region.

After photolithographic patterning using negative photoresist, metal-coating and lift-off define a hard mask for reactive ion etching of the waveguide patterns. For the pattern of Figure 6 (right), that step is followed by re-coating the substrate with positive resist for e-beam lithography. Patterns that connect the discontinuous waveguides are then written, including the tapered interaction region.

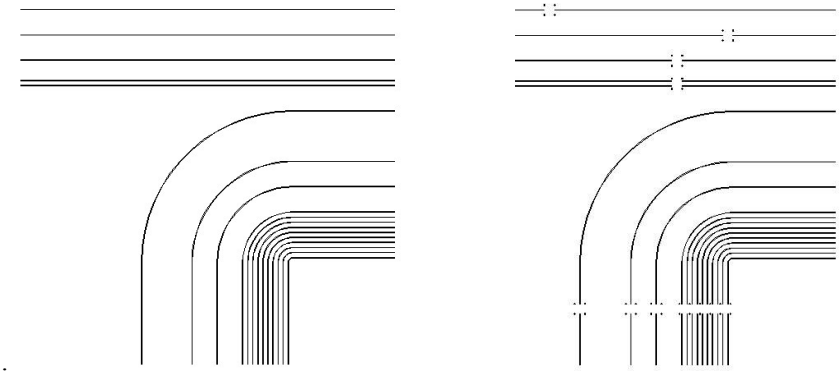

Figure 6 – Waveguide test patterns from photolithography mask. Left – continuous waveguides. Right – Discontinuous waveguides with breaks and alignment marks for writing interactions regions with e-beam lithography.

Another section of the test pattern photomask is shown below in Figure 7. Waveguides of varying bend radii contain discontinuities for e-beam lithography patterning, as described above. Alignment marks surround each discontinuity for registration within the e-beam write window. The pattern in Figure 7 is intended for writing micro-ring resonators as well as interaction regions. Continuous waveguides of the same dimension are included for baseline measurements.

Scanning electron micrographs of first fabricated waveguides are presented in Figure 7, right. The inner set of 10 micron-wide waveguides are spaced 100 microns apart, with radius of curvature increasing from 100 microns to 1 mm in 100 micron intervals.

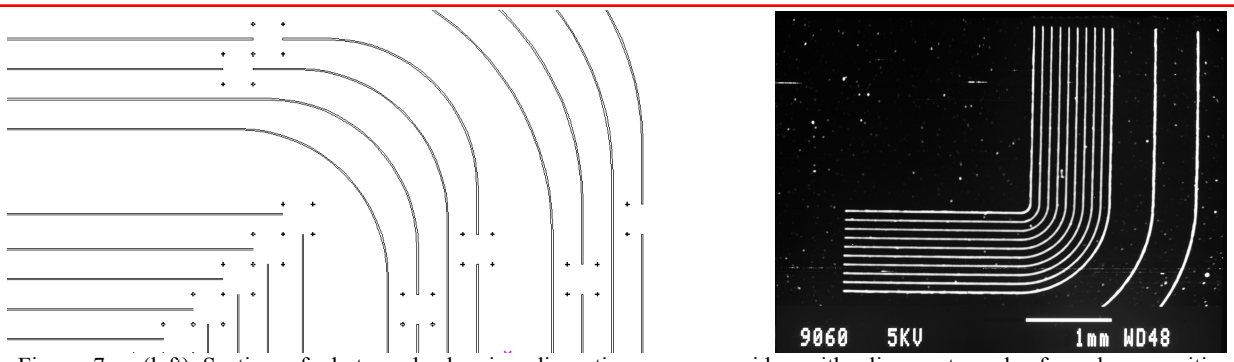


Figure 7 – (left) Section of photomask showing discontinuous waveguides with alignment marks for e-beam writing of interaction regions and ring resonators. (right) SEM image of fabricated silicon photonic waveguide. (right) SEM image of an alignment mark on SOI wafer, tilted view.

## 4. TAPERS

### 4.1 Fabrication

Figure 8 (top) is the design of the interaction region to be written by e-beam lithography. The waveguide (gray) is tapered to width 1 micron, over a distance of 25 microns. Si islands flank the tapers and narrow section separated by a gap. These islands are to be plated with Au in the last step. Figure 8 (bottom) shows an optical micrograph of this pattern written by e-beam lithography in positive resist. This pattern is to be coated with metal by e-beam evaporation, followed by lift-off in methylene chloride to form a hard mask for reactive ion etching of the gaps between the flanking silicon islands and the central silicon tapers and waveguide.

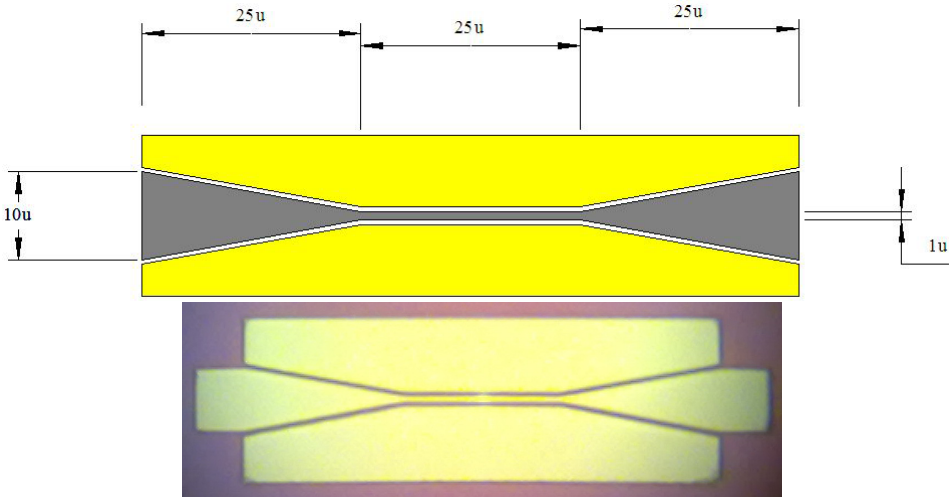


Figure 8 – (top) Drawing of the interaction region for e-beam lithography. (bottom) Optical image of the pattern written by e-beam lithography in positive resist.

## 5. INTERACTION REGION

Figure 9 presents results of 3D FDTD simulations that demonstrate the creation by the tapers of surface plasmons in the gap of the interaction region. The input silicon waveguide has 10 μm x 10 μm cross section on oxide. The fundamental mode is launched at this input. The waveguide then tapers to 1 μm width in the interaction region and the gap to the metal is 150 nm. The E-field is polarized horizontally, as required for exciting a SPP on the flanking metal surfaces. Fig. 9 (left) presents an end view of the interaction region together with the electric field intensity distribution. Fig. 9 (right) presents the top view. The high intensity in the gap shows that an SPP has been excited.

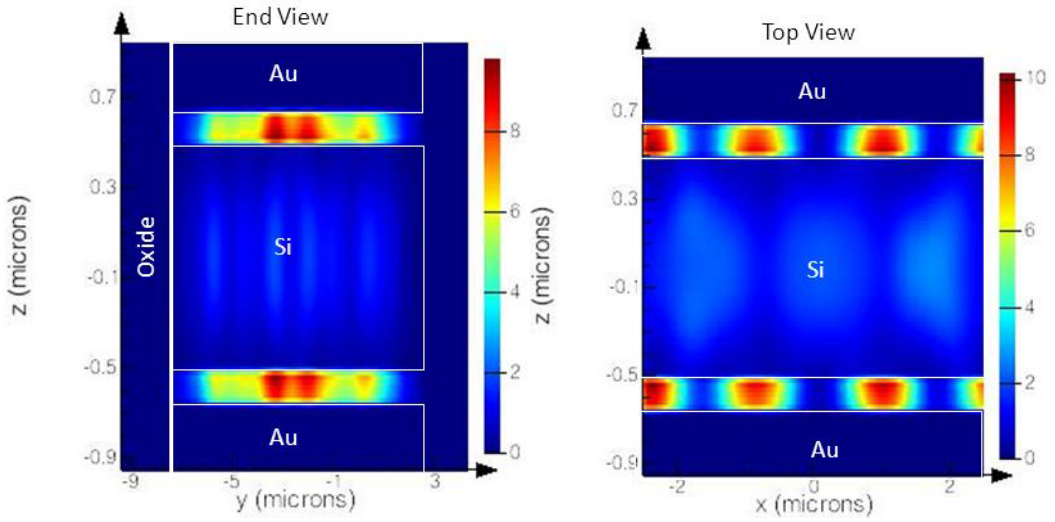


Figure 9- (left) 3D FDTD simulation showing excitation of the gap mode for our device structure, end view cross section. (right) top view.

Figure 10 (left) presents a plot of the transmitted power vs gap width, as determined from the FDTD calculations. When the width of the waveguide is below cutoff, transmission through the interaction region is only 20-30%. However, a sufficiently narrow gap allows excitation of an SPP, which effectively transmits power through the interaction zone. A gap width of ~100 nm seems ideal.

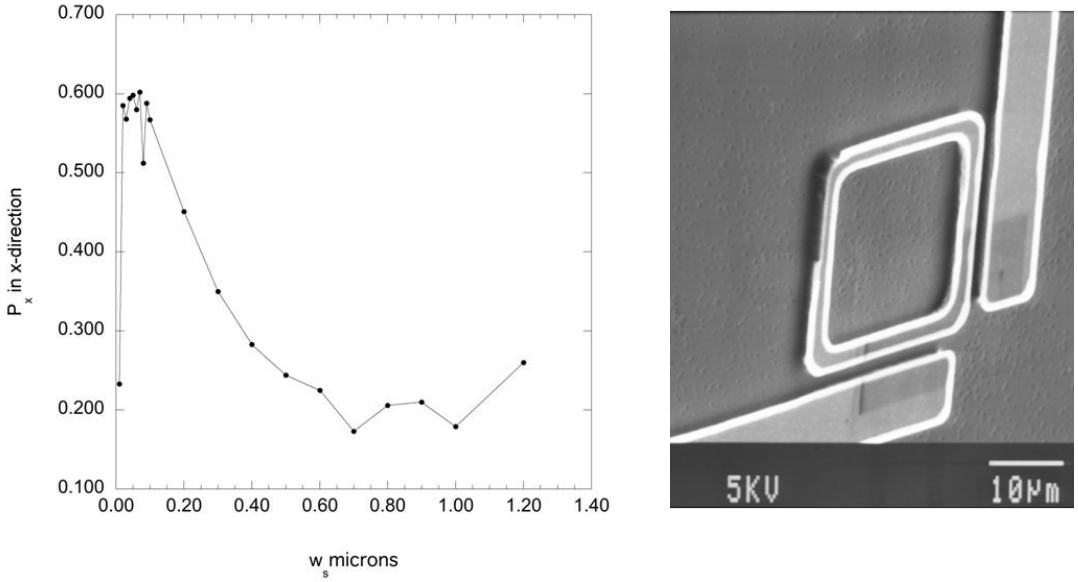


Figure 10 – Transmission as a function of gap width, when the waveguide width is below cutoff. (right) Fabricated micro-ring resonator, defined by optical lithography from the photomask, coupling two discontinuous waveguides.

We estimate for the necessary length of the interaction region using the Beer-Lambert law, $T = e^{-N\sigma x}$. We suppose a molecular radius of 10 nm, giving a molecular volume of $10^{-18}$ $cm^3$. For 100% concentration, this gives a concentration of $10^{18}$ $cm^{-3}$. Taking a healthy but not untypical molecular absorption cross section of $10^{-18}$ $cm^2$ gives $T = e^{-x}$ with x measured in cm. For an easily measureable change in transmittance due to molecular absorption of say 10%, we have $e^{-x} = 0.9$, or $x = -\ln(0.9) = 0.1$ cm. So an interaction region of length 1 millimeter seems appropriate, according to this rough calculation. SPP propagation length of several millimeters is reasonably expected for 3 micron wavelengths (0.4 eV)[1].

## 6. MICRO-RING RESONATOR

The requirement for the ring resonator is that it should have a circumference equal to an integer ($m$) number of optical wavelengths. For 3.4 micron wavelengths in silicon (n = 3.4), the circumference needs to be $3.4m/3.4 = m$ microns. The free spectral range FSR = $\lambda/m$ should be sufficiently large so that opposite ends of the spectrum are not simultaneously resonant in any one ring. This requirement favors small values of $m$. We require an FSR of 0.34 micron at 3.4 microns wavelength, so that the largest value of $m$ should be 10, giving a 10 micron circumference, or a diameter of 3 microns.

The width of the ring must be larger than the optical wavelength, but not so large as to allow transverse modes, which would lower the Q. Thus, the width should be approximately 1 micron at 3.4 microns vacuum wavelength. The Q must be at least 2500 so that each ring picks up just a single resolution channel. The maximum possible Q is $2\pi n/(\lambda\alpha)$, where $\alpha$ is the propagation loss in the ring material[6]. Assuming a comfortably large value for $\alpha$ of 0.1 $cm^{-1}$ gives a Q of 60000, showing that the 2500 requirement is actually rather modest.

Results of initial ring resonator fabrication are shown in Figure 10 (right). This particular micro-ring resonator was defined on the photomask. The corners have radius 3 microns and the 3 micron wide extended straight sections are designed to improve coupling with the waveguides by providing a longer interaction length. The micro-ring resonators to be defined by e-beam lithography will have widths of approximately 1 micron, with distinct channels defined by differences in diameter of tens of nanometers.

## 7. CONCLUSION

We report progress on design and fabrication of the enabling components for a SPP-based spectrometer-on-a-chip at wavelengths near 3.4 microns, which has low atmospheric absorption and where C-H,.N-H, O-H, C=O, $NH_2$, and C-N molecular vibrations occur. This region is hence especially suitable for sensing of chemical and biological threats.

## ACKNOWLEDGMENTS

This work was supported by Air Force Office of Scientific Research Phase I STTR award FA9550-11-C-0063 and grant FA9550-10-1-0030. J. W. Cleary would like to acknowledge support from the Air Force Office of Scientific Research (Program Manager Dr. Gernot Pomrenke) under contract number 12RY10COR.

## REFERENCES

[1] R. Soref, R. E. Peale, and W. Buchwald, "Longwave plasmonics on doped silicon and silicides," OPTICS EXPRESS **16**, 6507 (2008).
[2] R. E. Peale, O. Lopatiuk, J. Cleary, S. Santos, J. Henderson, D. Clark, L. Chernyak, T. A. Winningham, E. Del Barco, H. Heinrich and W. R. Buchwald, "Propagation of high-frequency surface plasmons on gold," J. Opt. Soc. Am. B **25**, 1708-1713 (2008).
[3] N. Feng and L. Dal Negro, "Plasmon mode transformation in modulated-index metal-dielectric slot waveguides," Optics Letters **32** (21), 3086-3088 (2007).
[4] G. Z. Mashanovich, M. M. Milosevic, M. Nedeljkovic, N. Owens, B. Xiong, E. J. Teo, and Y. Hu, "Low loss silicon waveguides for the mid-infrared," Optics Express **19** (8), 7112-7119 (2011).
[5] R. A. Soref, J. Schmidtchen, and K. Peterman, "Large single-mode rib waveguides in GeSi-Si and Si-on-$SiO_2$," IEEE J. Quantum Elec. **27** (8), 1971 (1991).
[6] J. Neihusmann, A. Voerckel, P. H. Bolivar, T. Wahlbrink, W. Henschel, H. Kurz, "Ultrahigh-quality-factor silicon-on-insulator microring resonator," Optics Lett. **29**, 2861 (2004).